optica

Quantum dot white LEDs with high luminous efficiency: supplementary material

SADRA SADEGHI,[1,+] BASKARAN GANESH KUMAR,[2,+] RUSTAMZHON MELIKOV,[2] MOHAMMAD MOHAMMADI ARIA,[3] HOUMAN BAHMANI JALALI,[3] AND SEDAT NIZAMOGLU[1,2,3,*]

1. Graduate School of Materials Science and Engineering, Koç University, Istanbul, 34450, Turkey.
2. Department of Electrical and Electronics Engineering, Koç University, Istanbul, 34450, Turkey.
3. Department of Biomedical Sciences and Engineering, Koç University, Istanbul, 34450, Turkey.
‡ Current Address: Department of Chemistry, PSR Arts and Science College, Sivakasi, India
+ These authors have contributed equally to this work.
**Corresponding author: snizamoglu@ku.edu.tr*

Puublished 12 July 2018

This document provides supplementary information to "Quantum dot white LEDs with high luminous efficiency," https://doi.org/10.1364/OPTICA.5.000793. In the first section, we provide the quantum yield optimization of red- and green-emitting QDs. The second section shows the structural and elemental characterization of synthesized QDs. In the third section, we provide the simulation algorithm and results for white light-emitting diodes (LEDs). In the fourth section, the fabrication method of PDMS polymeric lens is provided. The optical properties of the blue LED chip were demonstrated in the fifth section. In the sixth section, the properties of GB-based (Green/Blue) QD-LED are presented. In the seventh section, the simulation results of luminous efficiency (LE) and NTSC color gamut ratio were shown. The last section shows the optical properties of close-packed and solid-state LEDs.

1. Quantum yield optimization

A. Photoluminescence peak wavelengths of efficient red-emitting CdSe QDs

In the main text, we mentioned that during the QY optimization for red-emitting CdSe QDs, there were other points with different reaction times and temperatures, which have similar QYs with the selected point of 2 minutes reaction time at 300 °C. The photoluminescence peak wavelength of the synthesized CdSe QDs at 240 °C of reaction temperature and 60 minutes of reaction time was 657 nm with QY of 37%. The photoluminescence peak wavelength of the synthesized CdSe QDs at 260 °C of reaction temperature and 7 minutes of reaction time was 612 nm with QY of 35.5%, and the photoluminescence peak wavelength of the synthesized CdSe QDs at 300 °C of reaction temperature and 2 minutes of reaction time (our selected point) was 640 nm with QY of 38%. Moreover, the photoluminescence spectra of these points were shown in Figure S1.

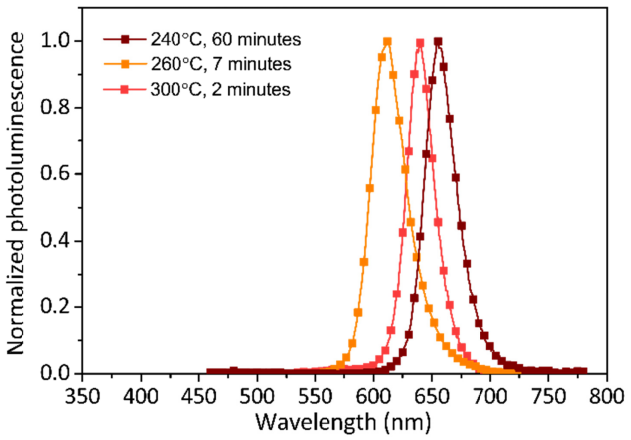

Fig. S1. The photoluminescence spectra of the synthesized red-emitting CdSe QDs with different reaction times and temperatures, which have similar QY with the selected point of 2 minutes reaction time at 300 °C.

B. Quantum yield and FWHM of QD structures

In the main text, we mentioned the optimization of red- and green-emitting QDs. The FWHM and QY of red-emitting CdSe, CdSe/CdS and CdSe/CdS/ZnS QDs were shown in Fig. S2. The FWHM of the QDs remained almost constant during the shelling process, which indicated the homogenous dispersion and growth of the synthesized QDs. For green-emitting QDs, the FWHM of CdSe core was significantly high, which was due to the initial surface state trap formation. The surface traps broadened the photoluminescence spectra of green-emitting CdSe QDs. Continuation of shelling process led to narrow FWHM, which passivated the surface traps. Moreover, the change in QY of the synthesized QDs in each step of shelling process was shown in Figure S2.

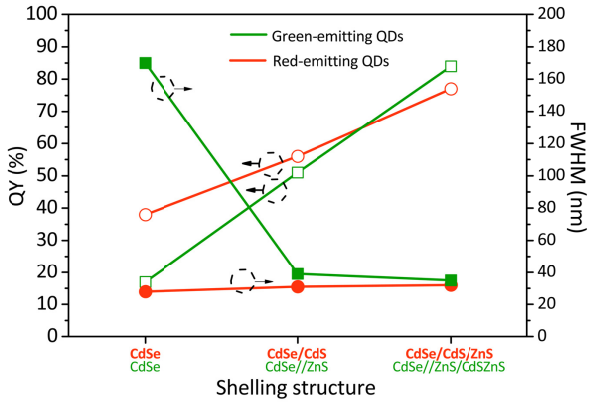

Fig. S2. Quantum yield (QY) and FWHM of red- and green-emitting QD structures.

C. The effect of CdS multiple shelling

We investigated the effect of different CdS and ZnS shelling and measured QY for each sample. Figure S3 showed the QY results for CdS and ZnS shelling (from 1 to 3 times) of red-emitting QDs. Our optimization confirmed that the red-emitting QD structure with only one shelling of CdS and ZnS showed the highest QY of 77%.

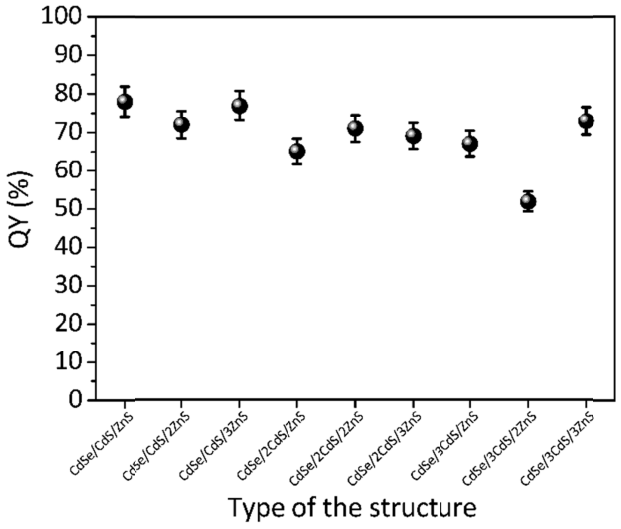

Fig. S3. The QY of red-emitting CdSe/CdS/ZnS QDs with different shell combinations.

2. Characterization

A. TEM

The structure and size distribution of the synthesized red- and green-emitting QDs were measured by transmission electron microscopy (TEM) (Figure S4). The red-emitting CdSe/CdS/ZnS QDs showed a size distribution of 6.23 ± 0.77 nm and the green-emitting CdSe//ZnS/CdSZnS QDs showed a size distribution of 5.89 ± 0.93 nm. The size distribution for each of the red- and green-emitting QDs were calculated by using 100 particles.

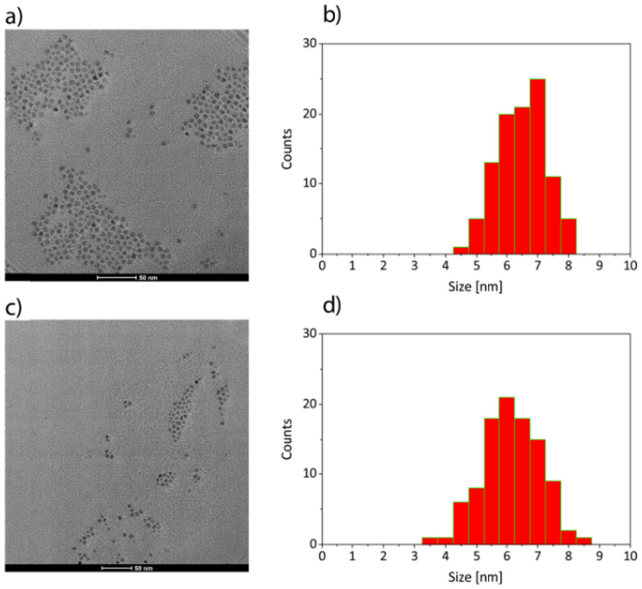

Fig. S4. (a) TEM images of red-emitting CdSe/CdS/ZnS QDs. (b) The size distribution of the red-emitting QDs. (c) TEM images of green-emitting CdSe//ZnS/CdSZnS QDs. (d) The size distribution of the green-emitting QDs. (Scale bar =50 nm)

B. SEM EDS

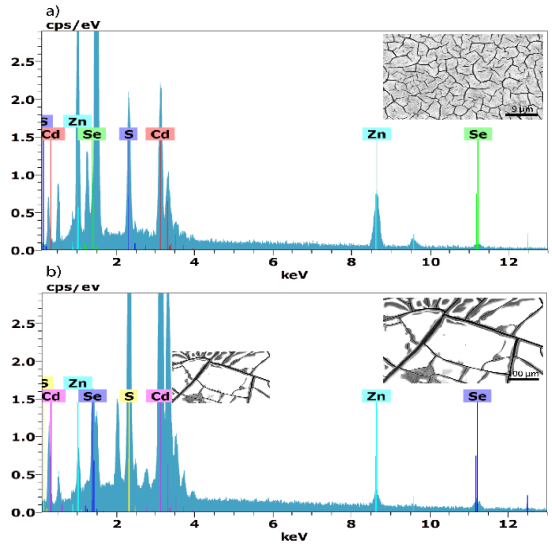

Fig. S5. The elemental composition for (a) red- and (b) for green-emitting QDs. Inset: The SEM image of the QDs sample dried on a glass substrate.

As mentioned in the main text, elemental analysis was performed on the red- and green-emitting QDs to investigate the presence of cadmium, selenium, zinc and sulfur in QD structures. The results showed that cadmium, selenium, zinc and sulfur elements are present in both red- and green-emitting QDs, respectively (Figure S5).

C. XRD

The XRD measurement was performed to investigate the structural analysis of the synthesized red- and green-emitting QDs. The diffraction pattern of CdSe, CdS and ZnS structures were shown in Figure S6 (lower panel). As mentioned in the main text, the peaks at 25°, 28°, 42°, and 57° confirmed the CdSe, CdS and ZnS cubic structures in Figure S6 (upper panel). The shift in some diffraction peaks (e.g. at 26°) was due to the lattice mismatch between core and shell [1].

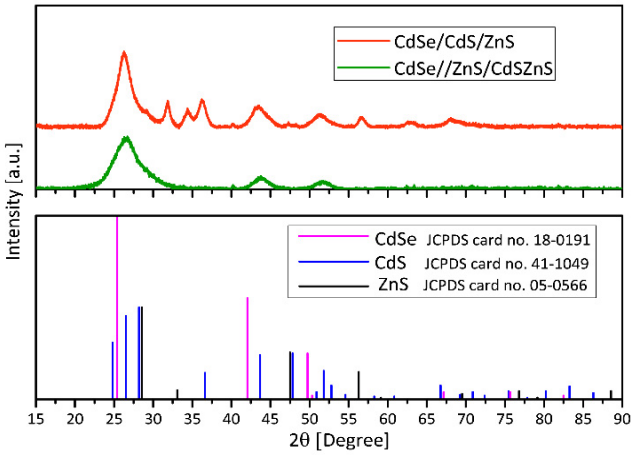

Fig. S6. XRD measurement of red- and green-emitting QDs. Upper panel showed the XRD pattern of red- and green-emitting QDs, and lower panel showed the diffraction patterns of the CdSe, CdS and ZnS cubic structures.

D. XPS

The XPS measurement was used to confirm the core/shell formation in both red- and green-emitting QDs. The change in binding energy of cadmium, zinc, selenium and sulfur indicated formation of new bonding between elements, which was due to the core and shell structure formation (Figure S7). At the same time, XPS measurement also confirmed the presence of cadmium, zinc, selenium and sulfur elements in red- and green-emitting QDs.

3. Simulation of quantum dot white LEDs

The calculation is based on the reference [2]. Shortly, the spectral overlap between the absorbance of the fluorophore and electroluminescence intensity of the pump results in photoluminescence of the fluorophore, where photons are absorbed and spontaneous emission occurs. In this process, incoming photon flux with power spectral density ($\overrightarrow{S_{in}(\lambda)}$) is absorbed by the fluorophore with absorption coefficient ($\alpha_i(\lambda)$). Total output power spectral density ($\overrightarrow{S_{out}(\lambda)}$) generated by combination of photoluminescence of the fluorophore and transmitted incoming photon flux. The matrix formulation presented in equation (1) takes into account reabsorption and inter-absorption processes where $\kappa_i(\lambda)$ corresponded to absorption ratio of electroluminescent pump by i_{th}

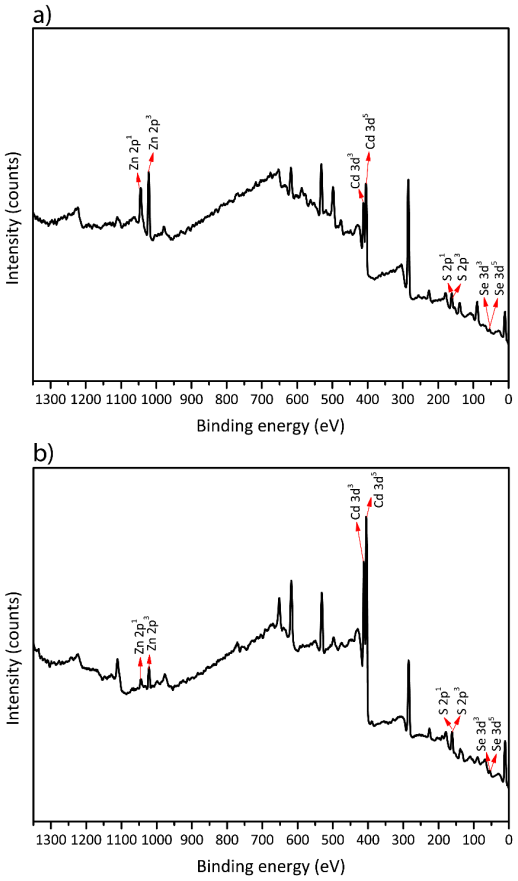

Fig. S7. The XPS spectrum of (a) red- and (b) green-emitting QDs

fluorophore. W_i corresponded to the emission strength, which showed the absorption of each fluorophore by electroluminescent pump scaled by QY meaning that only emission (radiative recombination) is considered. $M_{i,i}$ corresponded to the reabsorption of the i_{th} fluorophore and $M_{i,j}$ corresponded to inter-absorption between i_{th} and j_{th} fluorophore. $P_{j,n}$ corresponded to normalized spectral emission strength at n_{th} wavelength of the j_{th} fluorophore. $\bar{\bar{C}}$ was the spectral multiplication factor to the overall emission due to reabsorption and inter-absorption, which was the simplified form of the sum of infinitely many reabsorption and inter-absorption cycles.

$$\overrightarrow{S_{out}(\lambda)} = \overrightarrow{S_{in}(\lambda)} \exp\left[-\sum_j \alpha_j(\lambda) D_j\right] + \vec{W}^T \times \bar{\bar{C}} \times \bar{\bar{P}} \quad (1)$$

$$\kappa_i(\lambda) = \frac{\alpha_i(\lambda) D_i}{\sum_j \alpha_j(\lambda) D_j} \quad (2)$$

$$W_i = Q_i \int S_{in}(\lambda) \kappa_i(\lambda) \left\{1 - \exp\left[-\sum_j \alpha_j(\lambda) D_j\right]\right\} d\lambda \quad (3)$$

$$M_{i,j} = Q_j \int P_i(\lambda)\kappa_j(\lambda)\left\{1 - \exp\left[-\sum_j \alpha_j(\lambda)D_j\right]\right\}d\lambda \quad (4)$$

$$\bar{\bar{C}} = (I - \bar{\bar{M}})^{-1} \exp\left[-\sum_j \alpha_j(\lambda)D_j\right] \quad (5)$$

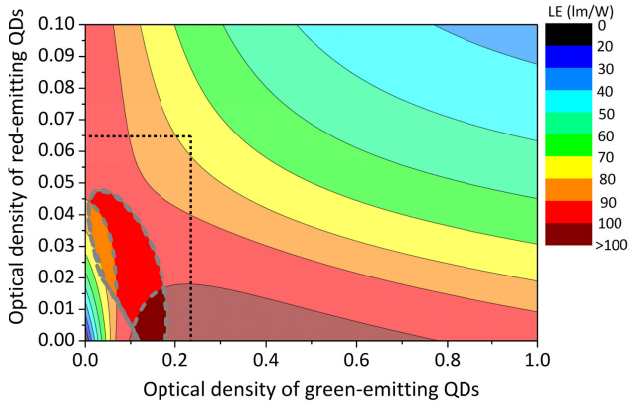

Fig. S8. The bright-dashed region showed the combination of red- and green-emitting QDs, which led to white light generation. The black-dashed rectangle indicated the specific area shown in Figure 4(e).

The matrix method described above with a built-in MATLAB code was used to simulate red- and green-emitting QDs to analyze the spectra of the color conversion LEDs. The EQE of the respective QDs are calculated by using electroluminescent pump spectra, QY, absorbance and photoluminescence of the respective QDs.

As mentioned in the main text, we simulated the LE values of LQD-LEDs based on different optical densities of red- and green-emitting QDs. The results were shown in color map of Figure 4(e) in the main text. In Figure 4(e), to better visualize the white region, the optical density ranges of [0, 0.22] for green-emitting and [0, 0.065] for red-emitting QDs were shown. The full color map of the simulated results for optical density ranges of [0, 1] for green- and [0, 0.1] for red-emitting QDs were shown in Figure S8.

4. PDMS polymeric lens fabrication

We designed and fabricated an aluminum mold to prepare the PDMS polymeric lens. The schematic of the curing process was explained in Figure S9 (a). The aluminum helped better thermal conductivity, which accelerated the curing process and prevented the bubble formation.

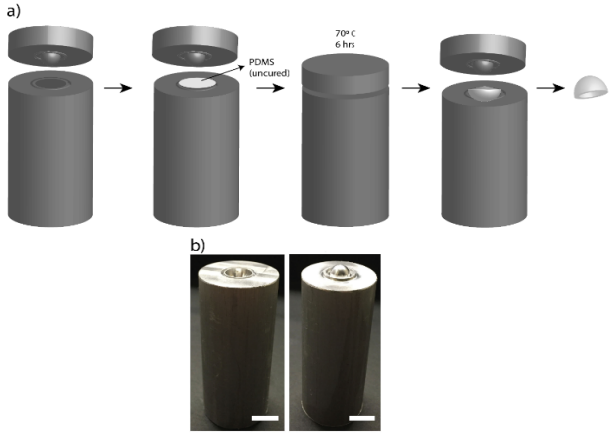

Fig. S9. (a) The schematic of lens fabrication procedure using the designed aluminum mold and PDMS. (b) (Left) the lower and (right) the upper part of the mold, which was placed on top of each other to fabricate the polymeric lens with hollow hemispherical shape. The scale bar is 1 cm.

5. The optical properties of blue LEDs

The optical properties of the blue LEDs, which were used in this study, were characterized (Figure S10).

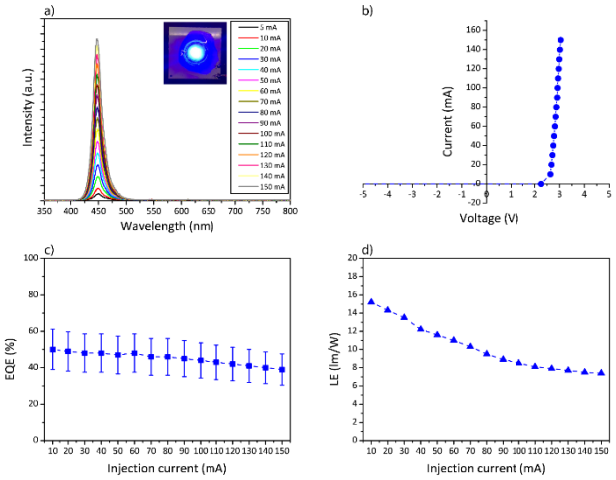

Fig. S10. (a) Intensity spectra of an exemplary blue LED chip at different injection currents from 5 to 150 mA. Inset: the photograph of the blue chip when the LED was turned on. (b) I-V curve of the blue LED. (c) The EQE of the blue LED chips at different injection currents from 10 to 150 mA. (n=4) (d) The luminous efficiency of a blue LED at different injection currents from 10 to 150 mA.

6. GB-based LQD-LED

The green-emitting QDs with the optical density of 0.13 was injected onto a blue LED. The combination of green emission and blue light generated a point with (x,,y) coordinates of (0.31, 0.39) in CIE 1931 color tristimulus, which was inside the white region (Figure S11).

The white region in CIE 1931 chromaticity coordinates were defined as follows by using the equations (6-8) [3]:

$$x' = \frac{y + 1.67x - 0.885}{1.9495} \quad (6)$$

$$y' = \frac{y - 0.607x - 0.109}{1.1648} \quad (7)$$

$$\frac{x'^2}{0.1339^2} + \frac{y'^2}{0.0944^2} \leq 1 \quad (8)$$

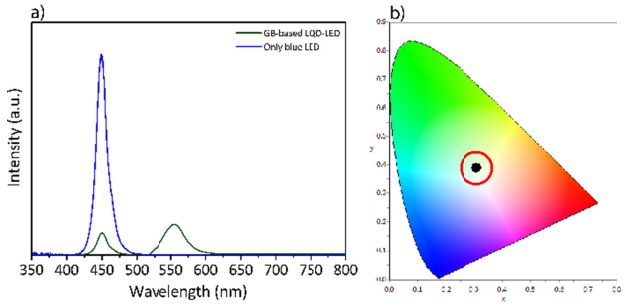

Fig. S11. (a) The spectrum of GB-based LQD-LED (b) The (x,y) tristimulus coordinates of GB-based LQD-LED in CIE 1931 chromaticity diagram.

7. The simulation results of color gamut, LE and CRI

As mentioned in the main text we performed a simulation in order to investigate the effect of PL peak wavelengths of the red- and green-emitting QDs on the NTSC color gamut ratio (Table S1). We selected a range of 510-580 nm and 580-660 nm for green- and red-emitting QDs, respectively. The step size was selected as 5 nm. Our simulation results showed that the NTSC gamut ratio of 104% was achievable with the PL peak wavelength of 515 nm for green-emitting QDs and the PL peak wavelength of 635-660 nm for red-emitting QDs (orange colored cells in Table S1). These results were shown in Figure S12-color map.

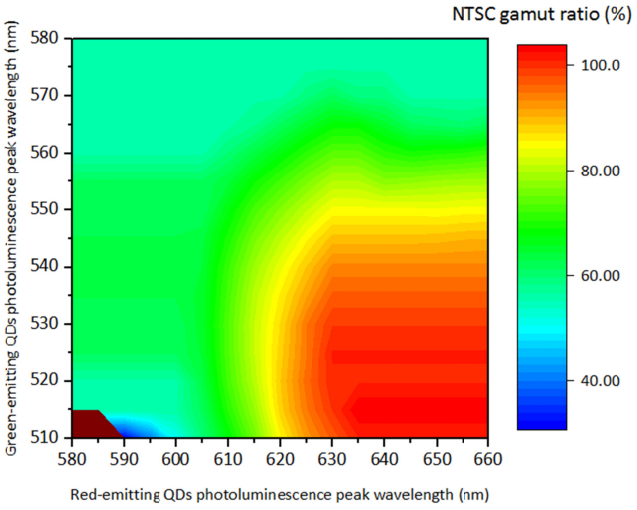

Fig. S12. The simulation that investigated the maximum NTSC gamut ratio by varying the photoluminescence peak positions of red- and green-emitting QDs.

We performed the similar simulation to investigate the effect of PL peak wavelength of red- and green-emitting QDs on LE of the generated white light. Our simulation results showed that by the PL peak wavelength of 555-560 nm for green-emitting QDs for all PL peak wavelengths of red-emitting QDs from 580 nm to 660 nm, max LE of 120 lm/W was achievable (orange colored cells in Table S2). These results were shown in Figure S13-color map.

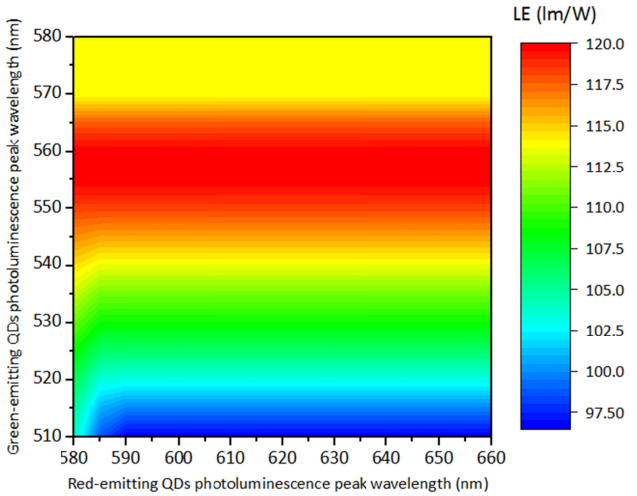

Fig. S13. The simulation that investigated the maximum luminous efficiency by varying the photoluminescence peak positions of red- and green-emitting QDs.

As we mentioned in the main text, we also simulated the dependence of CRI values with LE using the optical parameters of the optimized red- and green-emitting QDs. The results indicated that maximum LE of 80 lm/W with CRI of 84 was achievable using the optimized red- and green-emitting QDs (Figure S14).

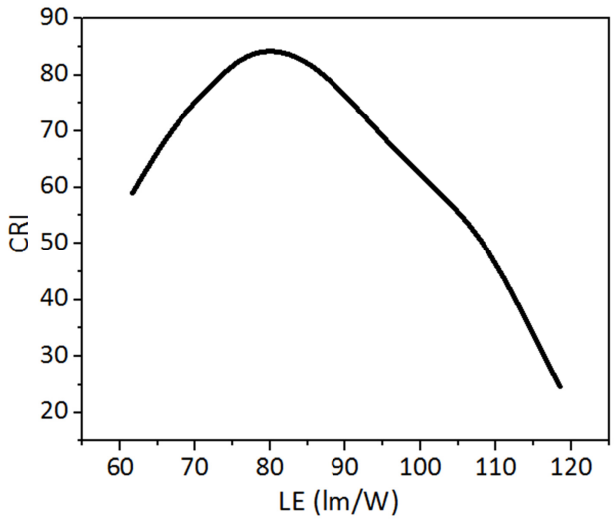

Fig. S14. The simulation of CRI-LE based on the photoluminescence and absorbance of the synthesized red- and green-emitting QDs.

8. The optical properties of liquid-state, solid-state and close-packed QD-LED structures

The optical properties of different types of QD-LED structures were calculated at different injection currents from 10-150 mA. The calculation of EQE was shown in equation (9) [4], in which K(λ) is the eye sensitivity function, $I_e(\lambda)$ is the color conversion spectra, I is the injection current (A) and V is the voltage (V).

$$EQE = \frac{LE}{LER} = \frac{\frac{\int_0^\infty I_e(\lambda)K(\lambda)d\lambda}{IV}}{\frac{\int_0^\infty I_e(\lambda)K(\lambda)d\lambda}{\int_0^\infty I_e(\lambda)d\lambda}} \quad (9)$$

The EQE, LE, and LER of the liquid-state, solid-state and close-packed QD-LED at different injection currents were shown in Figure S15.

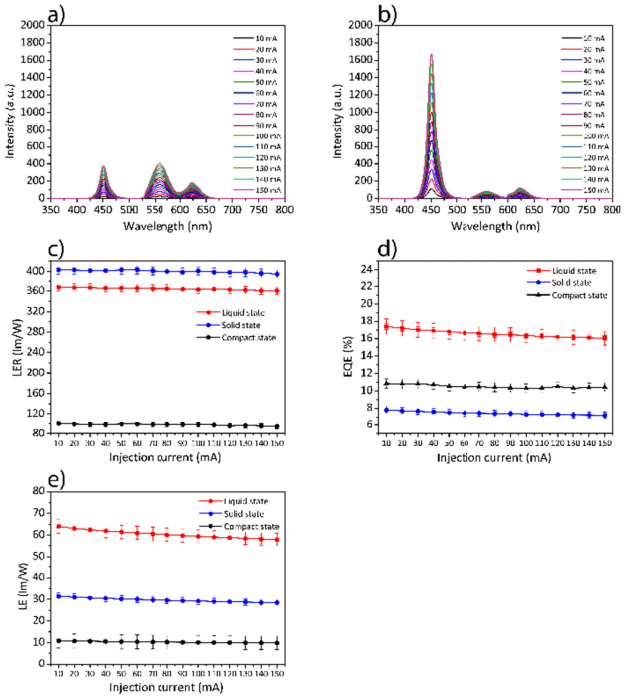

Fig. S15. The intensity spectra of (a) solid-state and (b) close-packed QD-LED at different injection current from 10 to 150 mA. (c) The luminous efficiency of radiation (LER) (d) The EQE, and (e) the luminous efficiency of different structures of QD-LEDs at different injection currents from 10 to 150 mA.

Table. S1. The simulation results of NTSC color gamut ratio with photoluminescence peak positions of red- and green-emitting QDs. The orange-colored cells showed the highest achievable NTSC gamut ratio (%).

The peak wavelength of green-emitting QDs (nm)	The peak wavelength of red-emitting QDs (nm)																
	580	**585**	**590**	**595**	**600**	**605**	**610**	**615**	**620**	**625**	**630**	**635**	**640**	**645**	**650**	**655**	**660**
510	--	--	31	40	51	59	67	75	85	92	97	101	101	101	101	101	101
515	56	56	56	56	56	62	71	78	88	95	99	104	104	104	104	104	104
520	56	56	56	56	56	63	72	80	89	96	101	101	101	101	101	101	101
525	61	61	61	61	61	65	73	81	88	95	101	101	101	101	101	101	101
530	61	61	61	61	61	65	73	81	87	95	99	99	99	99	99	99	99
535	63	63	63	63	63	65	73	80	86	92	97	97	97	97	97	97	97
540	63	63	63	63	63	64	72	78	84	89	94	94	94	94	94	94	94
545	63	63	63	63	63	64	70	76	81	85	89	89	89	89	89	90	90
550	61	61	61	61	61	61	67	73	77	81	85	85	85	85	84	85	85
555	61	61	61	61	61	61	64	69	72	76	80	80	77	78	78	79	79
560	56	56	56	56	56	56	60	63	67	71	74	74	71	69	70	71	72
565	56	56	56	56	56	56	56	58	62	65	68	68	65	62	61	60	62
570	56	56	56	56	56	56	56	56	56	59	62	59	59	56	56	56	56
575	56	56	56	56	56	56	56	56	56	56	56	56	56	56	56	56	56
580	56	56	56	56	56	56	56	56	56	56	56	56	56	56	56	56	56

Table. S2. The simulation results of luminous efficiency by varying the photoluminescence peak wavelengths of red- and green-emitting QDs. The orange-colored cells showed the highest achievable LE (lm/W).

The peak wavelength of red-emitting QDs (nm)

The peak wavelength of green-emitting QDs (nm)	580	585	590	595	600	605	610	615	620	625	630	635	640	645	650	655	660
510	104	99	97	97	97	97	97	97	97	97	97	97	97	97	97	97	97
515	105	101	100	100	100	100	100	100	100	100	100	100	100	100	100	100	100
520	107	103	103	103	103	103	103	103	103	103	103	103	103	103	103	103	103
525	109	106	106	106	106	106	106	106	106	106	106	106	106	106	106	106	106
530	111	109	109	109	109	109	109	109	109	109	109	109	109	109	109	109	109
535	113	111	111	111	111	111	111	111	111	111	111	111	111	111	111	111	111
540	115	113	113	113	113	113	113	113	113	113	113	113	113	113	113	113	113
545	116	116	116	116	116	116	116	116	116	116	116	116	116	116	116	116	116
550	118	118	118	118	118	118	118	118	118	118	118	118	118	118	118	118	118
555	120	120	120	120	120	120	120	120	120	120	120	120	120	120	120	120	120
560	120	120	120	120	120	120	120	120	120	120	120	120	120	120	120	120	120
565	118	118	118	118	118	118	118	118	118	118	118	118	118	118	118	118	118
570	114	114	114	114	114	114	114	114	114	114	114	114	114	114	114	114	114
575	114	114	114	114	114	114	114	114	114	114	114	114	114	114	114	114	114
580	56	56	56	56	56	56	56	56	56	56	56	56	56	56	56	56	56

REFERENCES

1. T.-L. Nguyen, M. Michael, and P. Mulvaney, "Synthesis of highly crystalline CdSe@ ZnO nanocrystals via monolayer-by-monolayer epitaxial shell deposition," Chemistry of Materials **26**, 4274-4279 (2014).
2. R. Melikov, D. A. Press, B. Ganesh Kumar, S. Sadeghi, and S. Nizamoglu, "Unravelling radiative energy transfer in solid-state lighting," Journal of Applied Physics **123**, 023103 (2018).
3. T. Erdem, S. Nizamoglu, X. W. Sun, and H. V. Demir, "A photometric investigation of ultra-efficient LEDs with high color rendering index and high luminous efficacy employing nanocrystal quantum dot luminophores," Optics Express **18**, 340-347 (2010).
4. H. C. Yoon, H. Kang, S. Lee, J. H. Oh, H. Yang, and Y. R. Do, "Study of perovskite QD down-converted LEDs and six-color white LEDs for future displays with excellent color performance," ACS applied materials & interfaces **8**, 18189-18200 (2016).